

Sedimentary trace element records over the last 200 kyr from within and below the northern Arabian Sea oxygen minimum zone

Cornelis H. van der Weijden^{a,*}, Gert-Jan Reichart^{a,b,1}, Bertil J.H. van Os^{c,2}

^a Department of Earth Sciences-Geochemistry, Faculty of Geosciences, Utrecht University, P.O. Box 80.021, 3508 TA Utrecht, The Netherlands

^b Alfred Wegener Institut for Polar and Marine Research, Biogeosciences, Am Handelshafen 12 (E), D-27570 Bremerhaven, Germany

^c TNO NITG, Department of Environmental Geosciences, Geochemical Research Group, P.O. Box 80.015, 3508 TA Utrecht, The Netherlands

Received 16 September 2005; received in revised form 26 April 2006; accepted 29 May 2006

Abstract

Two piston cores (PCs), containing two full glacial cycles, were retrieved at Murray Ridge. One core (PC463) contains sediment deposited at 920 mbsl within, the other (PC464) has sediment deposited at 1470 mbsl below the current oxygen minimum zone, OMZ ($O_2: \leq 2 \mu M$). Variations in the organic carbon (OC) content correlate well between the two cores; high OC contents correspond with periods of high insolation and are accompanied by a stable and intensive OMZ. The lithogenic fractions are similar and have a rather constant composition. The V, Mn, Co, Cu, Se, Zn and Sb contents in these fractions are in fair agreement with the values in standard shales (SS). The Ni content of the lithogenic fraction is higher than in SS due to its high content in the regional eolian input, and the Mo, Re and U contents are higher as a result of syngenetic and(or) diagenetic overprints. In both cores, Mn and Co have a negative, the other elements a positive correlation with OC. Four processes, contributing to sedimentary enrichment in trace elements, can be envisaged: 1) delivery, as minor or trace components, in hydrogenous and biogenic particles, 2) scavenging in the water column, 3) (partial) retention in the sediment during decomposition of host phases, 4) diffusion into the sediment across the sediment–water interface and subsequent immobilization in response to reduction or precipitation as sulfides. Vanadium, Mo, Re, and U were found to be clearly enriched, and Ni, Cu, Zn and Se to be possibly enriched as a result of these processes. Enrichment or depletion in trace elements in PC463 relative to PC464 was tested as a proxy for bottom-water oxygen (BWO) conditions during periods of maximum accumulation rates of organic matter. Only Mo, Re and Re/Mo appear to be unambiguous proxies for differences in depositional conditions between sites 463 and 464. Using these proxies, it was found that the OMZ expanded to at least the depth of site 464 from 155 to 135 ka.

© 2006 Elsevier B.V. All rights reserved.

Keywords: trace elements; redox; OMZ; organic matter; precession cycles; Arabian Sea

1. Introduction

A prominent feature of the modern northern Arabian Sea is its extensive and intense oxygen minimum zone (OMZ). Dissolved oxygen profiles (Fig. 1) show that the O_2 concentration drops to very low concentrations at a depth of 150 m and only starts to increase again below 1150 m. This intense OMZ is the result of high oxygen consumption rates by microbial mineralization of organic

* Corresponding author. Fax: +31 30 253 5302.

E-mail addresses: chvdw@geo.uu.nl (C.H. van der Weijden), reichart@geo.uu.nl (G.-J. Reichart), B.vanOs@geo.uu.nl (B.J.H. van Os).

¹ Fax: +31 30 253 5302.

² Fax: +31 30 256 4680.

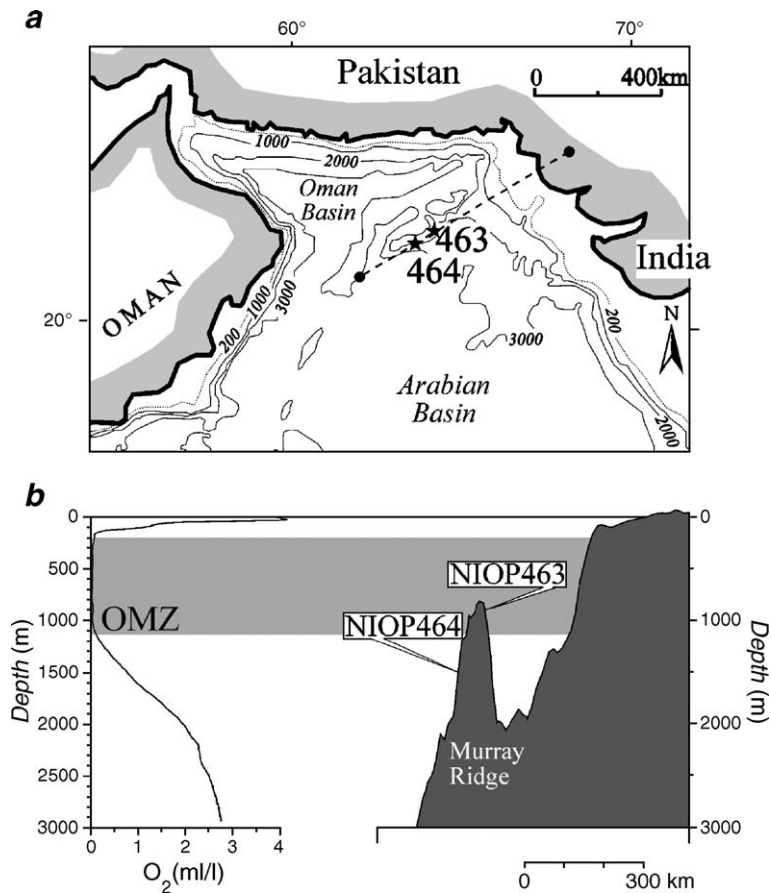


Fig. 1. a) Geographical positions of Murray Ridge stations 463 and 464 in the northern Arabian Sea; b) profile at Murray Ridge showing sea floor topography at stations 463 and 464, the extension of the present-day OMZ and dissolved oxygen concentrations (Van Bennekom and Hiehle, 1994).

matter (OM) exported from the euphotic zone and a moderate rate of intermediate water ventilation (Olson et al., 1993). The OMZ can be expected to change its intensity and (or) extent upon changes in export productivity (EP) and ventilation rate. Such changes occurred in the past, as concluded on the basis of profiles of sedimentary $\delta^{15}\text{N}$ (Altabet et al., 1995, 2002), deep-dwelling planktonic foraminifera (Reichart et al., 1998), organic matter, nickel and vanadium (Von Rad et al., 1999), manganese cycling (Schenau et al., 2002a) and benthic foraminifera (Den Dulk et al., 2000). Variations in the intensity of the OMZ have been ascribed to changes in the summer monsoon intensity (Schulz et al., 1998), the production of intermediate and deep-water masses (Schulte et al., 1999) and to deep convective mixing during periods of cold and intensified winter monsoon (Reichart et al., 1998). Temporal variations in OMZ intensity occurred at orbital and suborbital time scales. There is a close link between the cold phases of Dansgaard–Oeschger (DO) cycles and

breakdown of suboxic conditions in the OMZ (Reichart et al., 1998; Schulz et al., 1998; Altabet et al., 2002; Reichart et al., 2002). The occurrence of laminated OM-rich layers in a sedimentary record of the last 30 000 years showed that a stable OMZ existed during the past 7000 years and during warm interstadial events (Von Rad et al., 1999). In general, high productivity periods and concomitant enhanced OM burial is related to periods with an intensive OMZ, which in turn are related to precession minima (September, 35°N with an average time lag of ~ 7 kyr; Reichart et al., 1998) and (or) warm DO-events (Schulz et al., 1998; Reichart et al., 1998, 2002).

Fluctuations in redox-sensitive element concentrations in the sedimentary record can serve to reconstruct past variations in the bottom-water oxygen (BWO) concentration. Studies on trace metal behavior in dysoxic and anoxic bottom water have been conducted on numerous sedimentary records, such as for the Sea of Japan (Piper and Isaacs, 1995a, 1996), Gulf of California (Brumsack, 1989), California continental

margin (Dean et al., 1997), Black Sea (Brumsack, 1989; Colodner et al., 1995), Cariaco Basin (Jacobs et al., 1987; Dean et al., 1999; Yarincik et al., 2000; Lyons et al., 2003; Piper and Dean, 2003), Saanich Inlet (François, 1988; Calvert et al., 2001; Morford et al., 2001; Russell and Morford, 2001), northwestern Mexican Margin (Nameroff et al., 2002) and Peru and Chilean Margins (Böning et al., 2004, 2005).

In our study we will focus on and discuss concentrations of redox-sensitive and(or) sulfophile trace elements in two piston cores (PC) collected in the northern Arabian Sea during the Netherlands Indian Ocean Program (NIOP) in 1992. Since these PCs were taken within relatively close distance sedimentary fluxes can be expected to be quite similar. However, since one core is retrieved from within, the other from below the current OMZ, they are excellently suited to study differences in redox sensitive behavior. Elements considered in this study are antimony (Sb), cadmium (Cd), copper (Cu), manganese (Mn), molybdenum (Mo), nickel (Ni), rhenium (Re), selenium (Se), vanadium (V), uranium (U), and zinc (Zn). With the exception of Cd, Ni, and Zn, these elements can occur in different oxidation states in the aquatic environment. All these elements but Mn have a lower solubility under suboxic and(or) anoxic than under oxic conditions. As a result, the degree of loss (Mn) and enrichment (other elements) potentially reflect changes in BWO concentrations. We will investigate the applicability of the down-core distributions of these elements as records of changes in the extent and intensity of the OMZ in this part of the world ocean.

2. Regional setting

The modern Arabian Sea is very productive, largely due to southwest-monsoon driven upwelling of nutrient-rich intermediate water. The average export production of OM in the northeastern part of the Arabian Sea is on the order of $70 \text{ g C m}^{-2} \text{ yr}^{-1}$ (Van der Weijden et al., 1999). Ventilation of intermediate waters in the Arabian Basin occurs by O_2 -poor ($\sim 45 \text{ } \mu\text{M}$) Indian Ocean Central Water, with minor contributions by O_2 -rich Red Sea ($\sim 115 \text{ } \mu\text{M}$) and Persian Gulf Water ($\sim 160 \text{ } \mu\text{M}$) (Olson et al., 1993). The minimum O_2 concentration is $< 2 \text{ } \mu\text{M}$ (Van Bennekom and Hiehle, 1994) and the whole, 1-km thick, current OMZ can thus be called suboxic (Wignall, 1994).

3. Materials and methods

The two PCs studied in this paper were collected at Murray Ridge (Fig. 1) from within (PC463) and below the

OMZ (PC464) (Table 1). On board, the cores were cut into 1-m sections, which in turn were split lengthwise in half. One half was used for sampling, the other for core description and archive storage. Fixed-volume samples were taken with 10-cm spacing and their pore water contents determined by the weight loss after freeze-drying, on the basis of which dry and bulk densities could be calculated. Part of the samples were thoroughly ground in an agate mortar prior to an overnight digestion in an acid mixture of $\text{HClO}_4\text{--HNO}_3\text{--HF}$ in a tightly closed Teflon vessel on a sand bath that was kept at $105 \text{ } ^\circ\text{C}$. After subsequent evaporation of the solution, the residue was dissolved in 1 M HCl and the solution was used for analysis of Mg, Al, S, K, Ca, Ti, V and Mn by ICP-OES (ARL 34000) using international and in-house sediment standards as references. In general, the relative precision and accuracy of the results is better than 3%. The carbonate content was calculated from total Ca using a correction for clay-bound Ca: $\text{CaCO}_3(\text{sample}) = 2.5 \times (\text{Ca}_{\text{sample}} - (\text{Ca}/\text{Al})_{\text{clay}} \times \text{Al}_{\text{sample}})$ where $(\text{Ca}/\text{Al})_{\text{clay}} = 0.345$ (Turekian and Wedepohl, 1961; also the average of ratios in upper continental crust (Taylor and McLennan, 1985) and North American shale (Gromet et al., 1984)). For the analysis of trace elements, digestion was carried out as described, but the dry residue was dissolved in a 4.5% HNO_3 solution and measured by ICP-MS (Fisons Plasmaquad PQ2+). Three standard solutions, freshly prepared from commercial available single element stock solutions, were used for calibration. One standard solution (low concentrations) was measured after every seven samples to monitor and correct for drift, under the assumption of linear change. After drift correction, counts were corrected for variation in adjusted internal-standard (^{115}In , automatically added by the second channel peristaltic pump by which the analytes were introduced into the plasma) counts. Every fourteen samples a new calibration was performed. The isotope counts used in this study were of ^{59}Co , ^{60}Ni , ^{63}Cu , ^{66}Zn , ^{82}Se , ^{95}Mo , ^{114}Cd , ^{121}Sb , ^{187}Re and ^{238}U . Calibration was performed by taking into account natural abundances of the elements with respect to abundance in the crust and using a matrix of 63 major and minor elements. In this way, isobaric overlap of oxides and double charged ions is matrix compensated. The overall precision of the results is better than 10%. Samples older

Table 1

Geographical positions, water depths and current bottom water oxygen (BWO) concentrations for two coring sites as well as the lengths of the collected cores

Site number	Position (N)	Position (E)	Depth (m)	BWO (μM)	Length (m)
463	22°33.60'	64°03.25'	970	<2	14.3
464	22°15.00'	63°34.70'	1470	3.6	15.0

than 175 ka from core 464 have been excluded from further analyses because of apparent analytical problems.

The organic carbon (OC) content was determined as described in Reichart (1997) and Reichart et al. (1997). Relative precision and accuracy of the OC analyses were better than 3%.

The chronology of the Arabian Sea cores is based on tuning the Arabian Sea $\delta^{18}\text{O}$ record to that of a core from the Mediterranean (Fontugne and Calvert, 1992) using the sapropel chronology of Lourens et al. (1996). This chronology is based on correlation of the Mediterranean sapropel pattern to the astronomical record including a constant 3-kyr time lag. Keeping this time lag constant for the entire record enables comparison with other areas (Reichart et al., 1998). This independent age model produces an excellent correlation between characteristic phenomena in the sedimentary record in the two cores, although small offsets are inevitable (Fig. 2). Due to coring disturbances, sediment was lost at the top of both cores. The age of the base of the cores was established at 205 ka for PC463 and 225 ka for PC464.

4. Results

Element concentrations are given as supplementary data. Symbols of elements will be italicized when representing concentrations. The Al content of the terrigenous

fractions—calculated as the average of Al in the individual samples multiplied by a factor $100/[100 - \{(\sum \text{biogenic phases}) + \text{salt}\}]$ —is given in Table 2. In order to correct for dilution by terrigenous sediment components, element concentrations are often normalized by Al. A description of the use of Al as a divisor is given in the Appendix. Average values of Mg/Al , K/Al , Ti/Al and Fe/Al are similar in both cores and, with the exception of Mg/Al , compare quite well with those in standard shales (SSs).

Profiles of OC are presented in Fig. 2 and show that in both cores OC corresponds to the 35°N late summer insolation (Reichart et al., 1998). Henceforth, the precession related maxima in OC are numbered by their corresponding precession minimum (i.e. insolation maximum) from young to old, specified by IP 2 to 20. Corresponding peaks in OC values in core 464 are systematically lower than those in PC463, however two high OC intervals in PC464 show values similar to those in PC463, namely between 155 to 135 ka (IP14) and — for a relatively short interval — at about 170 ka (IP16).

The down-core profiles of trace element contents are shown in Fig. 3a-l. The Al-normalized contents of V, Mo, Cd, Re and U in PC463 are higher, and those of Mn and Co are lower or about equal in comparison to PC464. The normalized contents of Ni, Cu, Zn, Se and Sb are partly lower in PC63 and higher in PC464. With the exception of the one of Sb, the profiles in PC463 and

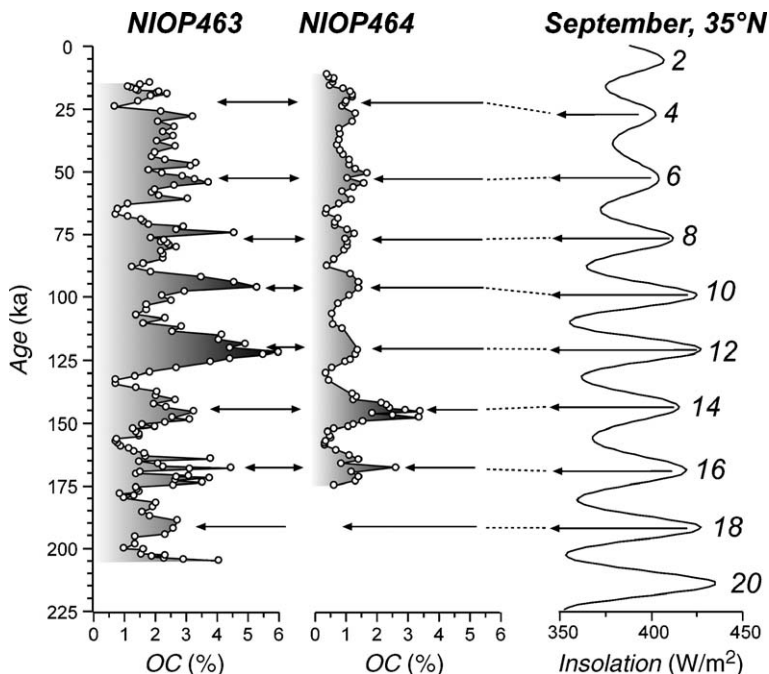


Fig. 2. Profiles of OC (data from Reichart, 1997). The age model is described in Reichart et al., 1998, the concomitant insolation curve in Laskar et al. (1993). Even numbers pertain to periods of maximum insolation (precession minima).

Table 2

Summary of data on the composition of world shale average (WSA; Wedepohl, 1971), post-Archean shales (p-AS; Taylor and McLennan, 1985), North Atlantic shale composite (NASC; Gromet et al., 1984) and average sediment at stations 463 and 464 on Murray Ridge

	WSA	p-AS	NASC	PC463	PC464 (normal)	PC464 (anomalous)
<i>Al</i> (%)	8.84	10	8.97	8.23 (0.47)	8.69 (0.55)	
<i>Ti/Al</i> (%/%)	0.055	0.06	0.054	0.064 (0.001)		
<i>Fe/Al</i> (%/%)	0.55	0.51	0.49	0.56 (0.04)		
<i>Mg/Al</i> (%/%)	0.18	0.13	0.19	0.45 (0.04)		
<i>K/Al</i> (%/%)	0.34	0.31	0.37	0.32 (0.01)		
<i>V/Al</i> (ppm/%)	15	15	–	15.4 (0.8)	18.1 (0.6)	20.5 (3.5)
<i>Mn/Al</i> (ppm/%)	96	85	56	89 (3)	81 (4)	76 (3)
<i>Co/Al</i> (ppm/%)	2.1	2.3	2.9	2.4 (0.1)	2.9 (0.3)	2.5 (0.2)
<i>Ni/Al</i> (ppm/%)	8	5.5	6.5	14.4 (0.9)	16.5 (1.3)	20.8 (2.6)
<i>Cu/Al</i> (ppm/%)	5.1	5.0	–	5.0 (0.6)	5.7 (0.3)	7.8 (0.9)
<i>Zn/Al</i> (ppm/%)	11	8.5	–	12.1 (0.8)	14.8 (0.9)	15.5 (1.5)
<i>Se/Al</i> (ppm/%)	0.07	–	–	0.10 (0.02)	0.10 (0.03)	3.8 (1.8)
<i>Mo/Al</i> (ppm/%)	0.29	0.1	–	0.7 (0.3)	0.4 (0.1)	2.5 (1.8)
<i>Cd/Al</i> (ppm/%)	0.09	–	–	0.014 (0.06)	0.105 (0.25)	0.35 (0.27)
<i>Sb/Al</i> (ppm/%)	0.17	–	0.23	0.19 (0.02)	0.19 (0.02)	0.3 (0.1)
<i>Re/Al</i> (ppb/%)	0.02	–	–	0.5 (1.2)	0.8 (0.7)	0.6 (0.3)
<i>U/Al</i> (ppm/%)	0.42	0.31	0.30	0.8 (0.2)	0.8 (0.2)	1.5 (0.9)

The latter values are based on the statistics of the data set (*Al* through *K/Al*) or derived by extrapolation of plots of *X/Al* (*V/Al* through *U/Al*) versus *OC/Al*. The graphically derived intercept values obtained by standard linear regression of *y* on *x* are given with a confidence interval $\pm 2\sigma$ (bracketed values). The values derived for PC464 (anomalous) are for samples within the age intervals (155–135 ka) with an alleged expanded OMZ. The Al content is calculated on a (carbonate+pore-water salt+OM+opaline silica) - free basis.

PC464 generally show changes synchronous with major peaks in the precession related OC maxima (IP events 2 to 20, Fig. 2). The profiles of Mn show maxima in between these OC maxima. Smaller scale rapid oscillations are probably related to higher frequency climate changes such as the DO cycles (Reichart et al., 1998; Reichart and Brinkhuis, 2003; Reichart et al., 2004).

The baselines of the profiles in both cores show a pattern of generally decreasing and/or increasing *Al*-normalized contents which corresponds with the abrupt changes in sedimentation rates visible in the profiles of mass accumulation rates (MARs) (Fig. 4). The highest peaks in the MAR profiles occur in the intervals 185–135 ka, 90–60 ka and 20 ka–subrecent.

5. Discussion

Sediment can be divided based on its origin into two main groups: (1) terrigenous material, and (2) marine material. The latter can be subdivided again, based on its mode of formation in biogenic (carbonates, opal, OM) and hydrogenous (mainly authigenic inorganic oxides, carbonates, or sulfides) material. The discussion will be structured accordingly.

5.1. Terrigenous fraction

Several overviews of the average composition of standard shales (SSs) have been published that might

serve as reference for the terrigenous fraction of marine sediment (Table 2). The average values of Al calculated for PC463 and PC464 are slightly lower than the shale values, which suggests that sediments at both stations are diluted with a phase—most likely quartz—devoid of Al as well as trace elements. The profiles of *K/Al* and *Ti/Al* for the two stations have nearly identical average values and patterns (Fig. 5), confirming that sedimentation at the two stations was similar. *Ti/Al* is slightly higher than in SSs, which is most likely due to the distinctly different lithological units on the bordering continents. The profile of *Mg/Al* shows a trend of increasing values from the oldest ages (core bottom) to ~135 ka, then a decrease till ~120 ka, after which the values increase again to the most recent ages (core tops). Superimposed on this glacial–interglacial variability, changes on a precession time scale can be seen (Fig. 2). The profiles of *Fe/Al* (Fig. 5) show no such trends and fluctuations more likely result from early-diagenetic processes. Average values of *Mg/Al* and *Fe/Al* in the two cores are identical, but *Mg/Al* is significantly higher than in SSs. These higher *Mg/Al* values are probably due to input of dolomite and possibly palygorskite dust from central Arabia during periods of high aridity (Sirocko et al., 2000) and dolomite dust from the Persian Gulf area during periods of low sea level stands (Reichart et al., 1997). By and large, it can be concluded that the terrigenous fraction at sites 463 and 464 has a quite uniform composition showing similar changes over time, which is in line with their close proximity.

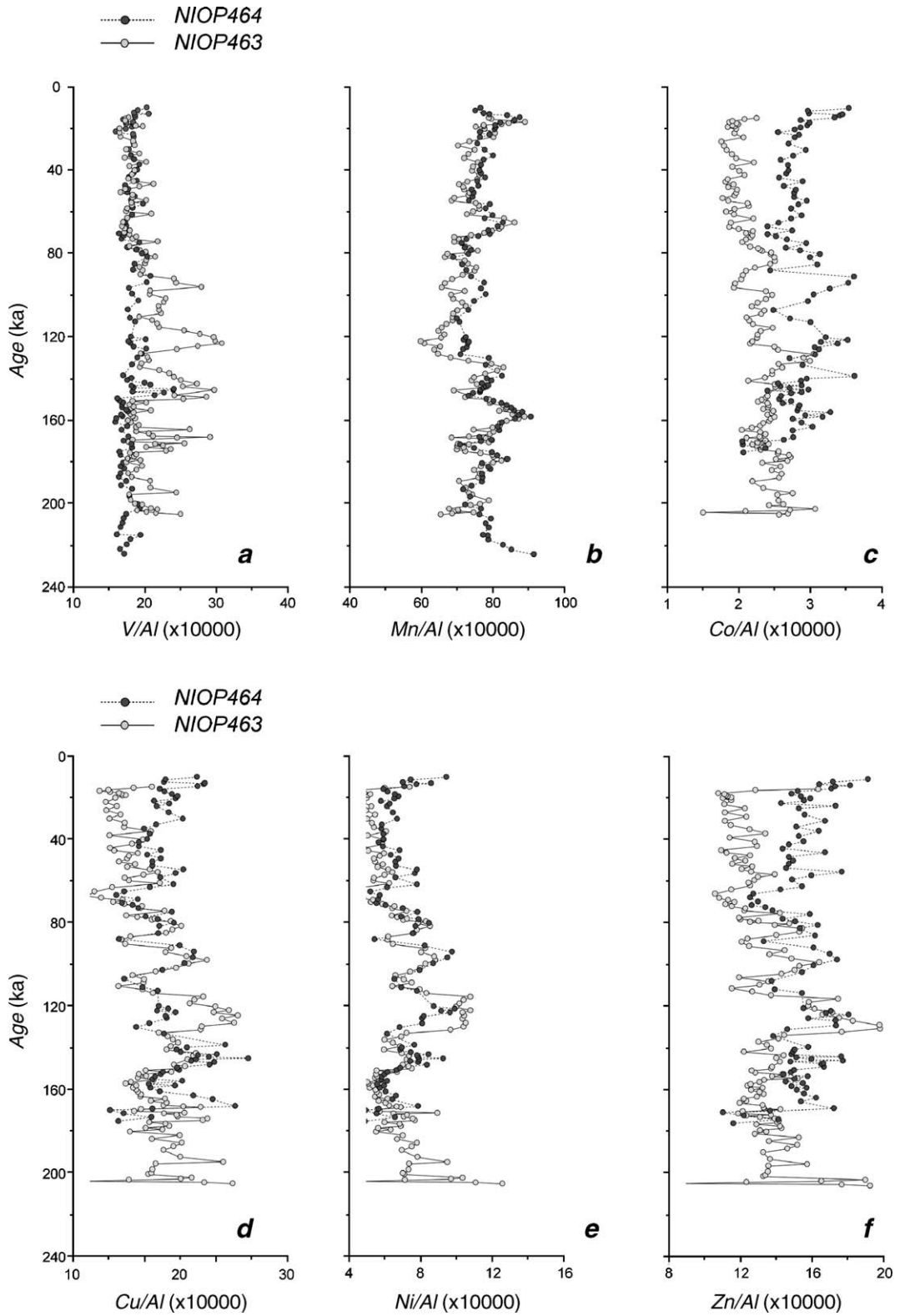


Fig. 3. Profiles of Al-normalized trace element concentrations (raw data in supplements).

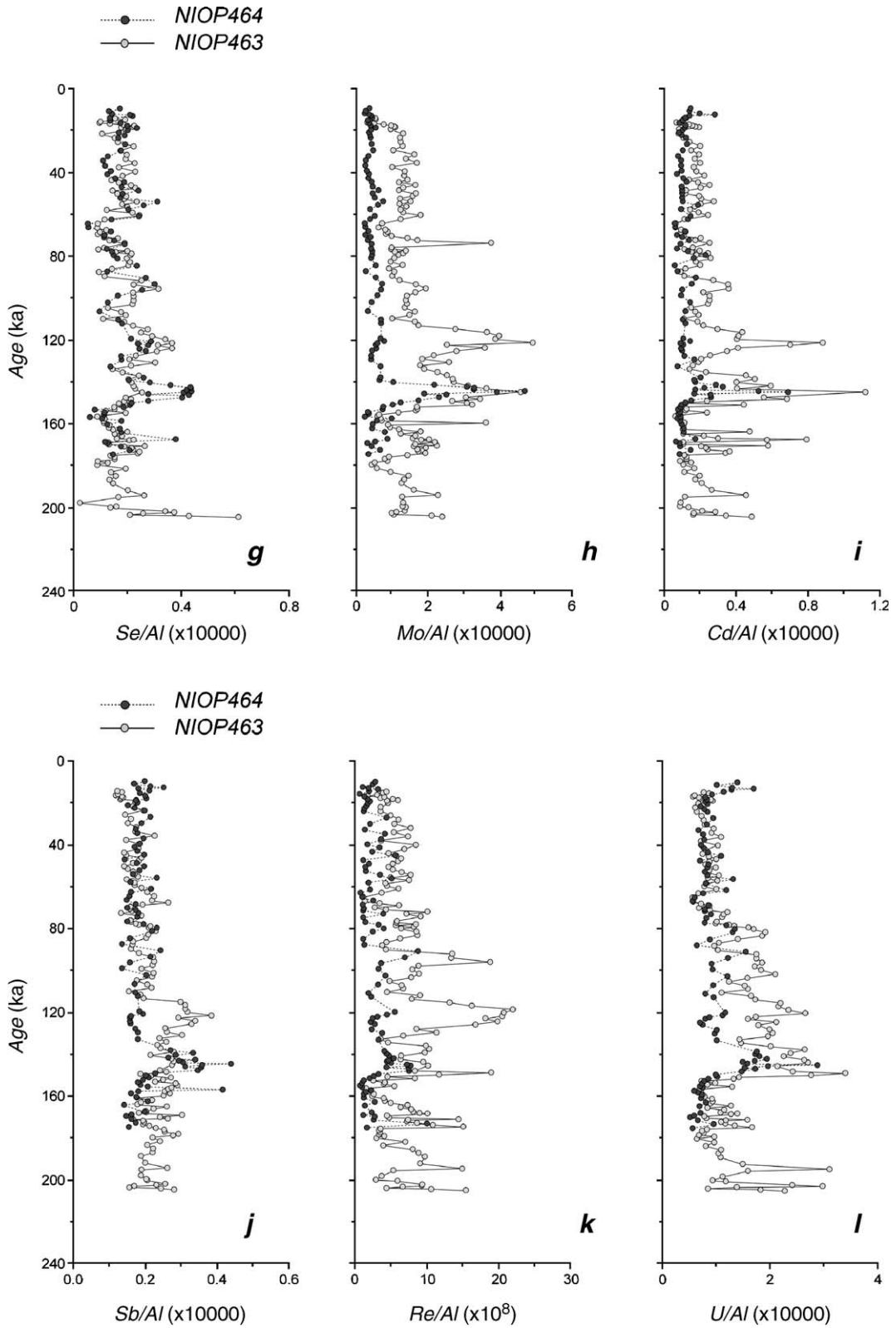


Fig. 3 (continued).

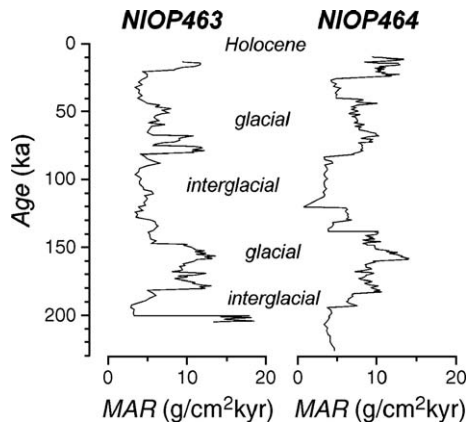


Fig. 4. Profiles of mass accumulation rates (MAR) (data in supplements).

Diagenetic, post-depositional, dissolution or formation of hydrogenous phases primarily depends on OM decay. Biogenic phases other than OM are practically

free of trace elements and no reduced hydrogenous components form in the absence of OM. Therefore, the intercept values of plots of X/Al — where X represents a trace element — against OC can be used to estimate the trace element contents of the terrigenous fraction, $(X/Al)_{\text{terrigenous}}$ (Eq. (A.2)). These intercept values are summarized in Table 2. For PC464, a separate column ('anomalous') is added for the values calculated for the periods 155–135 ka (IP14) and ~170 ka (IP16). For V , Co , Zn and Cd , the values are lower in PC463 than in PC464(normal), and of Ni , Cu , Zn , Se , Mo and U in PC464(normal) than in PC464(anomalous). The Al -normalized values for Ni , Zn , Mo , Re and U are also still higher than in SSs as a result of syngenetic and(or) diagenetic overprints. Because the terrigenous fractions in PC463 and PC464 are very similar in composition, one would expect the intercept values in plots of X/Al versus OC to be approximately equal. The $(X/Al)_{\text{terrigenous}}$ values in PC463 and PC464(normal) are indeed similar

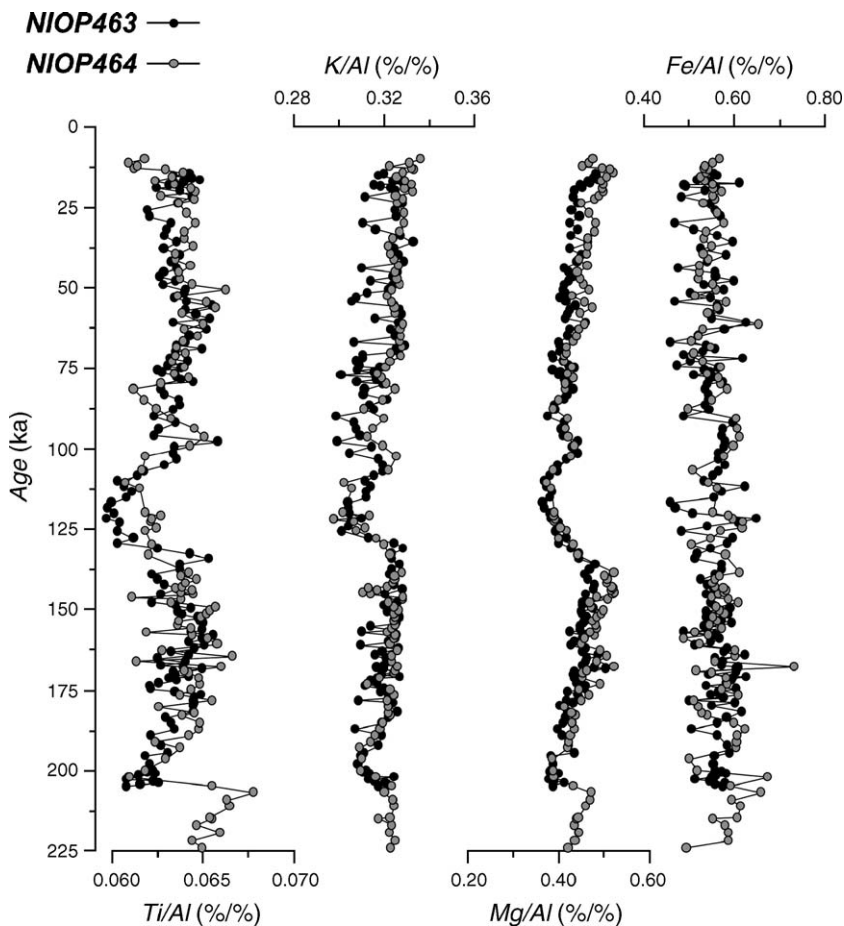


Fig. 5. Profiles of Al -normalized Mg , K , Ti and Fe as a function of age for PC463 and PC464. Data for PC464 were published earlier in Reichart et al., 1997.

(Table 2), with the exception of V, Cd and Zn. In the anomalous, OM-rich, sections of PC464 the values for Ni, Cu, Se and Mo are significantly higher than in the rest of PC464. In these anomalous sections ratios for V, Ni, Cu, Zn, Se, Mo and Cd are also higher than those in PC463 although this core generally has a higher OM content than PC464. The $(X/Al)_{\text{terrestrial}}$ values in PC463 and PC464(normal) show for Mn, Co, Cu, Se, and Sb a fair agreement with their values in SS. The Ni content, on the other hand, is higher than in SS, which is in keeping with previously suggested high atmospheric deposition of Ni into the Arabian Sea (Chester et al., 1991). Higher values of *Al*-normalized *Mo*, *Re* and *U* are most likely the result of syngenetic and/or diagenetic enrichment.

5.2. Marine fraction

The marine fraction of the sediment consists primarily of carbonates (PC463: $37 \pm 7\%$; PC464: $44 \pm 5\%$), organic matter (PC463: $2.26 \pm 1.08\%$; PC464: $1.14 \pm 0.64\%$) and biogenic silica (BC(boxcore)463: $\sim 3\%$; BC464: $\sim 2.5\%$; Van der Weijden and Van der Weijden, 2002). In addition hydrogenous phases are common sediment constituents.

The *OC* profiles at both stations (Fig. 2) are in phase, indicating that the productivity at these stations covaried. The accumulation rates of *OC* (CARs) in these cores are primarily controlled by surface water productivity, which in turn corresponds with monsoon-induced upwelling intensity (Reichart et al., 1998). The different amplitude of the *OC* profiles can be caused by the 500-m shallower water depth and enhanced preservation of *OM* at station 463 because of its position within the OMZ (Van der Weijden et al., 1999). Sinninghe Damsté et al. (2002), explained time-equivalent high CARs at the two stations (median peaks at 168, 147 and 52 ka) by a temporarily extended OMZ. High CARs at station 463 and at the same time much lower CARs at station 464 (at 123 and 95 ka) represent an OMZ similar to today's; low CARs at both stations (e.g. at 20, 75, 110 and 158 ka) correspond with low productivity, and thus also a much weaker OMZ. With an OMZ similar to today's and assuming that *OM* fluxes at the two sites were approximately equal, the average preservation of *OM* at site 464 would be about half that at site 463.

A plot of calculated *pyrite-S* versus *OC* (Fig. 6) shows the relation between these components. When *S* values at $OC > 2\%$ are excluded, ratios are similar to those of normal-marine sediments, because most of them plot within the range for these sediments as discussed by Berner (1984). The lower than normal *pyrite-S* values at

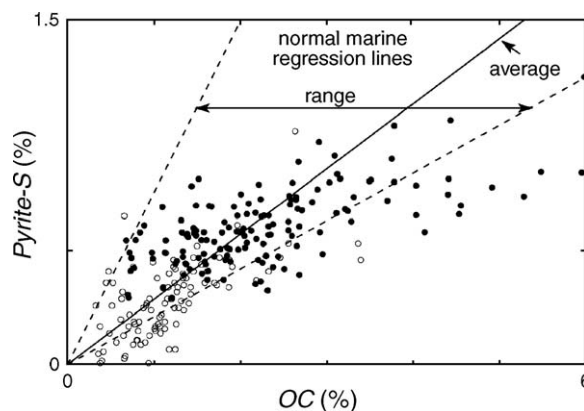


Fig. 6. Scattergram of *pyrite-S* versus *OC* for PC463 and PC464. The *pyrite-S* values were calculated from *bulk-S* by adopting: $pyrite-S \approx 0.9 \times bulk-S - 0.1$ for PC463, within the current OMZ, and $pyrite-S \approx 0.83 \times bulk-S - 0.14$ for PC464, below this OMZ (Schenau et al., 2002b). Linear curve fittings: $pyrite-S = 0.098 \times OC + 0.38$ ($R^2 = 0.43$) for PC463 and $pyrite-S = 0.21 \times OC + 0.02$ ($R^2 = 0.46$) for PC464. For comparison, the correlation for normal-marine oxygenated sedimentary conditions is shown (Berner, 1984). *Bulk-S* values for PC464 are from Reichart et al. (1997) and for PC463 from this work.

relatively high *OC* in PC463 (and in a few cases in PC464) could result from Fe limitation for pyrite formation under conditions of intense oxygen depletion (Schenau et al., 2002b). Scatter plots of *bulk-S* against *bulk-Fe* showed a good relation with the *S/Fe* ratio of pyrite in PC464 (Reichart et al., 1997) but not in PC463. However, similar patterns in profiles of both cores of *pyrite-S* and *Fe** (Fig. 7a,b) suggest that they still primarily reflect variations in pyrite content.

5.2.1. Trace-element baseline concentrations and climate change

As discussed in Section 4, the baseline concentrations of *Al*-normalized trace element profiles (Fig. 3) reflect climatic change on a time scale larger than that of precession. This might be caused by the export of previously deposited material from shelf and upper slopes during periods with a low sea-level stand, remobilizing reduced solid phases and — assuming general circulation and ventilation patterns equal to today — the OMZ descended about 100 m. In addition, the more arid glacial climate enhanced dust and reduced fluvial transport from the continent. During warm and wet periods the situation is reversed, with higher sea levels during interglacials. For that reason, the transition from glacial to interglacial (Fig. 4) can be expected to have affected long-term trends in trace element profiles. In general, shelf and upper-slope sediments store trace elements during high and become sources for these elements during low sea-level stands. If

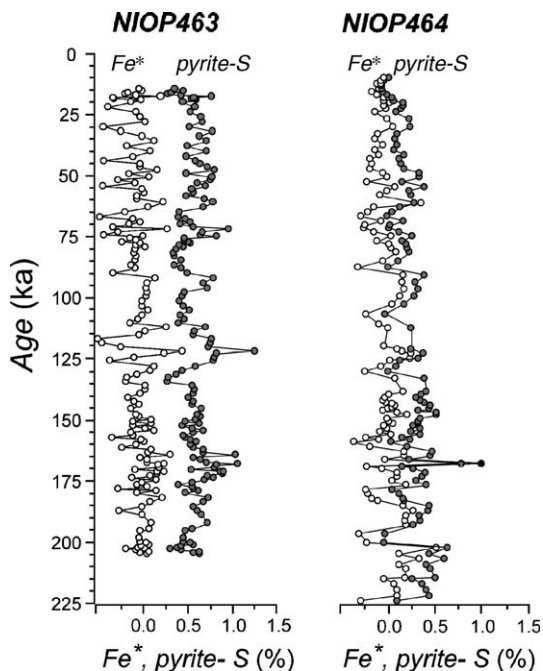


Fig. 7. Profiles of *pyrite-S* and Fe^* in PC463 (a) and PC464 (b). Fe^* was calculated by $Fe^* = \text{bulk-Fe} - 0.56 \times Al$, where the factor 0.56 represents $(Fe/Al)_{\text{terrestrial}}$ derived for the two cores (Table 2). In quite a number of cases the calculated values of Fe^* are negative, indicating that the factor 0.56 is too high. When a factor 0.44 (Schenau et al., 2002b) is used, the Fe^* values become positive, but this lower factor was derived in a sequential extraction step. Algebraically, the patterns are equivalent. The profiles visualize the similarity of the profiles of *pyrite-S* and Fe^* in each core, evidence of the presence of pyrite and variation of its content.

so, the differences in the baseline trends of element contents between PC464 and PC463 might be related to the position of site 463 within and that of site 464 below the OMZ.

5.2.2. Transport of trace elements to the sediment

Apart from transport in the lithogenic fraction, there are two important carriers of trace elements to the sediment: 1) Mn and Fe oxides (MFO), and 2) OM. In oxygenated surface water, Mn and Fe oxides are stable, both phases carrying incorporated trace elements such as Co, Ni, Zn, Cu, Mo, V, and other trace elements when settling at the ocean floor. Upon transit through an intense OMZ or deposition on the SWI under very low BWO conditions, reductive (partial) dissolution of MFO (Saager et al., 1989; Schenau et al., 2002a; Brumsack, 2006) takes place. Manganese and ferrous ions present in the OMZ (additionally acquired from previously oxic slope sediments) will be oxidized again below the OMZ (Schenau et al., 2002a) and the newly formed oxides will settle to the ocean floor adding to the oxidation

capacity of the sediments. The fresh oxides may eventually incorporate or adsorb trace metals (Brumsack, 2006). The decrease of dissolved Mn and Fe from within to below the OMZ, measured in profiles at a station in the proximity of sites 463 and 464 (sta. 7, Saager et al., 1989), is on the order of maximal 6 nM (Mn) and 4 nM (Fe). Assuming that this can be attributed to formation of MFO and considering that the concentration of trace elements in marine MFO such as ferromanganese nodules (which often have very long exposure time to bottom waters) is only a few per cent (mostly present in the birnessite phase), this will hardly effect dissolved trace metal concentrations. Indeed, the concentrations of Ni, Cu, Zn and Cd (sta. 7, Saager et al., 1992) continue to increase with depth across the lower boundary of the OMZ. Currently at station 463 hardly any Mn oxide (~0.007%) is present at the SWI and Fe oxide (top value ~0.55%) is consumed at a depth of 20 cm below the SWI, while at station 464 all Mn oxide (top value ~0.14%) is consumed at 5 cm and Fe oxide (top value ~0.28%) at 25 cm below the SWI (Van der Weijden et al., 1999). Taking this all together, the contribution of fresh MFO to the trace metal concentrations can be assumed to amount to a few ppm at most.

Organic matter plays an important role 1) as carrier and scavenger of trace elements to the sediment, and 2) in diagenetic enrichment (or depletion) in trace elements (Fig. 8). Live plankton needs trace elements for growth. After its decease, plankton may lose part of these trace elements (Collier and Edmond, 1984; Fisher and Wente, 1993). On the other end, faecal pellets produced in the food web reportedly have higher trace element concentrations than present in the zooplankton diet (Fowler, 1977), partly a result of co-ingestion of inorganic material. Scavenging depends on seawater concentrations and sorption affinities of dissolved species, on surface area and surface reactivity of settling particles, and on transit time. In fact, the largest part of OM is carried to the ocean floor as faecal pellets. Although reactivity of these pellets might be high, their settling velocities are larger than of loose or aggregated (marine snow) planktonic debris, resulting in limited time for scavenging of trace elements. Trace elements associated with settling OM may become liberated again upon oxic (in oxygenated water column) and suboxic (in OMZ with an intensely O_2 -depleted water column) decay of OM (Hong et al., 1995; Shaw et al., 1990). When the OM flux to the sediment is small, not only the residual OC but also the enrichment in trace elements will be small. In combination with BWO concentrations, deposited OM sets the stage for down-core redox zones. Berner (1981) distinguished three sedimentary redox zones: 1)

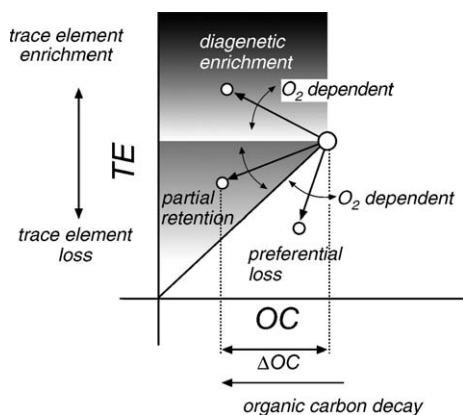


Fig. 8. Schematic representation of scenarios leading to loss or enrichment in trace element concentration upon degradation of organic matter (OM) at and below the sediment–water interface (SWI). In this scenario, the bottom-water oxygen (BWO) concentration is a key factor controlling the depths of the induced redox boundaries (cf. Meyers et al., 2005), which in turn affects the solubility of trace elements. At low BWO levels, the down-core boundaries from oxic to suboxic and suboxic to anoxic conditions are situated close to the SWI. In contrast, these boundaries lie deeper under oxygenated bottom water (BW). Release and (partial) escape to the BW of associated trace elements causes a negative, whereas sorption, precipitation and burial results in a positive trace element enrichment (TE). Under the assumption that OM flux to the ocean floor at stations 463 and 464 was not very different, oxic degradation of OM at station 464 (below the present-day OMZ) causes a relatively large decrease in organic carbon (OC) (Van der Weijden et al., 1999).

oxic, where O₂ is respired in the microbial degradation of OM, 2) suboxic, where nitrate, manganese and iron oxides (in that order) are used as electron acceptors in the microbial decomposition of OM, and 3) anoxic, where breakdown of OM is microbially mediated by reduction of sulfate into sulfide. Trace elements liberated after OM decomposition partly diffuse into the BW or are (partly) immobilized in the major sedimentary redox zones in accordance with their redox-sensitive and/or sulfophile character. Conversely, when concentrations of trace metals are higher in bottom water than in pore water (PW), diffusional enrichment in trace metals will occur. To which degree this enrichment happens depends on the depth of the redox boundaries below the SWI, the MAR, bioturbation depth, and the concentration differences, together establishing the diffusional concentration gradients. Within an intensive OMZ, bioturbation is limited to shallow depth (presently <0.1 cm at station 463 with bioturbation depth ~1 cm; Van der Weijden et al., 1999), causing a very shallow oxic–suboxic boundary in the sediment. In sediment deposited below the OMZ oxygen, exposure of OM plays an important role, bioturbation reaches deeper, and the oxic–suboxic boundary is located

deeper (currently, ~2 cm at site 464; with bioturbation depth ~7 cm; Van der Weijden et al., 1999).

5.2.3. Response of trace elements to changes in redox potential

The redox potential (Eh) of the sediment is determined by the degree of reduction of the major oxidants: oxygen, nitrate, Mn and Fe oxides, and sulfate. Current Eh –pH values (shipboard punch-in measurements with platinum and glass electrodes against a calomel reference electrode, calibrated with Zobell solution for Eh and NIST-standard pH solutions) in boxcores (BCs) changed from +115 mV and pH 7.45 (at 1 cm) to –0.44 mV and pH 7.23 (at 31 cm) at site 463 and from +140 mV and pH 7.35 (at 1 cm) to –10 mV and pH 7.43 (at 26 cm) at site 464. These values are indicative of suboxic conditions with reduction of Mn and Fe oxides in the top thirty centimeters, while down-core the Eh values decreased to the more negative values typical for sulfate reduction with the concomitant strong H₂S smell. Trace elements respond primarily to changes of redox conditions with a sequence of reduction descending the Eh ladder, with highest values in the oxic and lowest values in the anoxic zone. The positions of the trace elements on the Eh ladder (in this case based on a mix of observations reported by Calvert and Pedersen, 1993; Piper and Isaacs, 1995a,b; Thomson et al., 2001; Nameroff et al., 2002) indicate the sequence of their reduction and precipitation. For the trace elements in this study the inferred order of immobilization is V, (Se), U, and Re in the suboxic zone and Se, Mo, Cu, Cd, Zn, Ni in the anoxic(sulfidic) zone). In the oxic zone, metals usually associated with Mn oxide (for instance Co, Ni, Cu, Zn, Mo) and/or Fe oxide (for instance V), are considered to be immobile, but once liberated by reductive dissolution of MFO in the suboxic zone, sulfophile metals may, after downward diffusion, precipitate in the anoxic zone. The same holds for sulfophile elements liberated by decomposition of OM in the suboxic zone. Another possibility is that liberated elements are temporarily immobilized by sorption on reactive phases and become sulfidized when, by progressive burial, they enter the sulfate reduction zone. Additionally, diffusion across the SWI into the sediment and subsequent immobilization can be expected for dissolved elements with a high concentration gradient between BW and PW at the depth of immobilisation set by their Eh dependence. Based on this redox scheme, V, Re, U and Mo are the most likely candidates for enrichment, their solubility decreasing sharply when they are reduced from a high to a lower oxidation state or when they are immobilized as sulfides (Böning et al., 2004).

5.2.4. Relations between trace-element contents and organic matter

Trace element contents of the marine fraction (X^*) are calculated according to Eq. (A.3). The so derived X^* and OC data are plotted (Fig. 9) for periods with high OC contents, corresponding with periods of high northern hemisphere summer insolation (Fig. 2). It can be expected that $X^* \rightarrow 0$ when $OC \rightarrow 0$ (Eq. (A.5)). This extrapolation was used previously to derive $(X/Al)_{\text{terrigenous}}$ but — in some cases — failed to fully correct for syngenetic and diagenetic overprints. The slopes in the figures for the selected data sets (Fig. 9) are similar to those based on the complete data sets (not shown). The scatter in the plots of the selected data for PC463 is large ($R^2 < 0.5$) for all elements but Mn, Zn and Re, whereas in PC464 less scatter ($R^2 > 0.5$) is present for Ni, Se, Mo, Cd, and Sb. Taking into account the overall low coefficients of determination, it has to be concluded that there is no fixed relation between X^* and residual OC.

In PC464 slopes are steeper than in PC463 for Mn^* (negative), Ni^* , Cu^* , Zn^* , Se^* and U^* . These steeper slopes can result from more efficient decomposition of OM at station 464 in combination with — at least partial — retention of trace elements that were carried by this OM to the ocean floor (Fig. 8). Partial trace element retention might also play a role for the other elements in which the slopes in 464 are equally or less steep than in PC463 (V^* , Mo^* , Cd^* , Re^*), which implies that the original observed slopes in PC464 should be even more gentle. Better preservation of OM at station 463 would explain the overall difference between the cores.

According to Schenau et al. (2002a), dissolved Mn is removed from the suboxic OMZ and carried as oxide to the underlying oxic water column. Consequently, Mn enrichment is expected at station 464 compared to station 463. When plotted against OC, the loss in Mn at station 464, however, seems to exceed the loss at station 463 (steeper slope). Such a discrepancy might be due to a better retention of liberated

Mn under diagenetic conditions. The loss in Mn during deposition of the anomalous section of PC464 plots on the same (less steep) regression line as the losses in PC463. This suggests that during these time slices the OMZ was expanded till at least the depth at station 464.

Instead of a comparison of the slopes of the regression lines for all IPs, a comparison can be made on the basis of the differences in X^* and OC between the data for PC463 and those for PC464 for individual precession-related productivity maxima (Table 3). The rationale for such a comparison is that OC degradation (ΔOC) drives loss/enrichment in trace metals (Fig. 8), rather than the ultimately preserved OC. Negative values of ΔX^* and negative slopes of $\Delta X^*/\Delta OC$ indicate that X^* is higher in PC 464 than in PC463. Although ΔX^* depends on the levels of the X^* values, a small ΔX^* value (e.g. ΔSe^*) strongly suggests that X^* was not lost during diagenesis (cf. Fig. 8). The negative values of ΔCo^* , ΔNi^* , ΔCu^* and ΔZn^* for IP4–10 might be a result of enrichment by scavenging of these elements by Mn oxides formed below the OMZ (Hlawatsch et al., 2002; Schenau et al., 2002a; Brumsack, 2006) and their (partial) retention during subsequent diagenesis (Fig. 8). The positive values of ΔV^* , ΔMo^* , ΔCd^* , ΔRe^* and ΔU^* may be caused by loss upon oxic diagenesis or — more likely — by enrichment by diffusional enrichment and subsequent precipitation under conditions of low BWO. Clearly, shifts in $\Delta X^*/\Delta OC$ for the individual IPs are not equal, meaning that it is not only the lower OC in PC464 that causes the offsets of the data points (Fig. 9) for the cores. For all elements, the shifts for IP14, comprising data represented by PC464 (anomalous), are highest.

5.3. Bottom-water conditions during insolation maxima

Records of redox-sensitive elements are often used to reconstruct past variations in OMZ intensity (e.g. Reichart

Fig. 9. Scattergrams of X^* against OC in PC463 (black dots) and PC464 (open circles). The data were obtained as follows: First, OC background values (0.7% for PC463 and 0.35% for PC464) were subtracted from the original OC data. Then, the mean values of $(OC - \text{background})$ were determined. Next, the above-mean values of $(OC - OC_{\text{background}})$ for each of the maximum insolation periods (even numbers in Fig. 2) were averaged as well as the concomitant X^* values. Finally, these average X^* values were plotted against the corresponding average original OC (a-1). Each datum point corresponds to the number of the insolation maximum (Fig. 2), where the time slices (in ka) with peaks in OC were 34–18 (~IP4), 61–34 (~IP6), 80–72 (~IP8), 101–91 (~IP10), 128–120 (~IP12), 152–139 (~IP14) and 175–163 (~IP16). As a consequence of the way in which X^* was derived, intercepts of the X^* versus OC plots have a zero value. The concomitant X^* values were calculated by $X^* = X_{\text{total}} - X_{\text{terrigenous}} = Al \times \{(X/Al)_{\text{total}} - (X/Al)_{\text{terrigenous}}\}$ (cf. Eq. (A.3)). Assuming that the terrigenous components have the same trace element content throughout PC464, the $(X/Al)_{\text{terrigenous}}$ values derived for PC464 (normal) (Table 2, column 6) were used to calculate X^* for the whole core. The values of $(X/Al)_{\text{terrigenous}}$ [ppm/%], selected from Table 2, were: 88 (Mn), 15 (V), 29 (Co), 14.4/16.5 (Ni 463/464), 5 (Cu), 12 (Zn), 0.1 (Se), 0.3 (Mo), 0.09 (Cd), 0.19 (Sb), 0.0005 (Re), 0.4 (U). The linear fits of the data represent classical linear regression. With the exception of those for Mn^* and Co^* , all slopes are positive. Also plotted are the planktonic contributions. The planktonic trace element contents (in ppm; Piper, 1994; Piper and Isaacs, 1995b) are: V (3), Co (1), Ni (7.5), Cu (11), Zn (110), Se (3), Mo (2), Cd (12), Sb (0.5), Re (0.001) and U (1); Mn (2.6) (Collier and Edmond, 1984); Re (0.001) (estimated). On the basis of the Redfield formula for composition of plankton, these values were converted as follows: $X_{OC} = 2.8 \times X_{\text{plankton}}$.

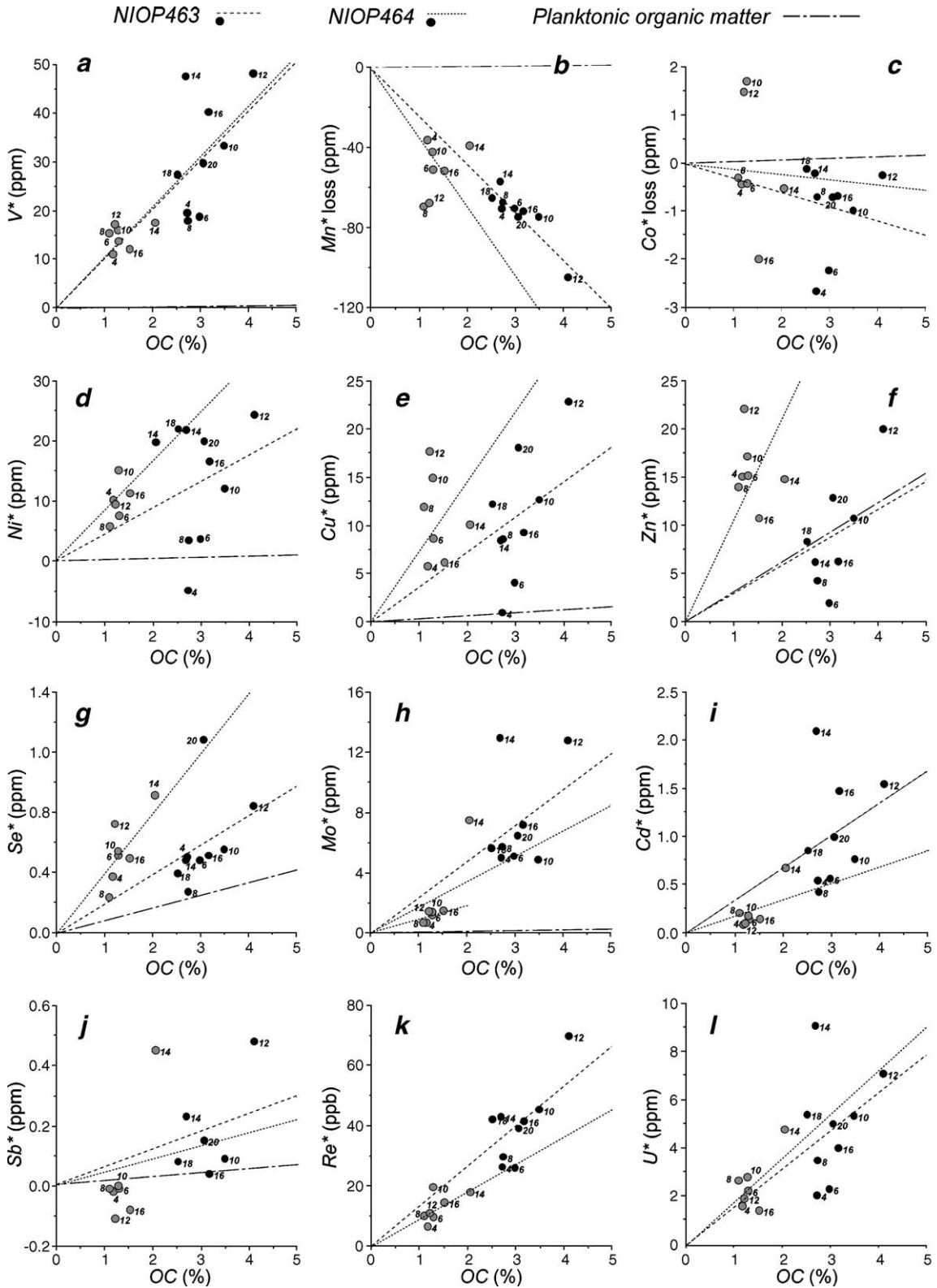


Table 3

Differences in trace element (all in ppm but for Re^* in ppb) and concomitant OC contents (%) in PC464 relative to PC463 as well as the slopes of $\Delta X^*/\Delta OC$ (ppm(or ppb)/%) for seven insolation phases (IP4–16; cf. Fig. 9a–l)

IP→	4	6	8	10	12	14	16
ΔOC	1.55	1.69	1.65	2.21	2.88	0.64	1.65
$\Delta Mn^* \Delta Mn^*/\Delta OC$	-34	-19	2.1	-32	-37	-18	-20
	-22	-11	1.3	-15	-13	-28	-12
$\Delta V^* \Delta V^*/\Delta OC$	8.5	5.1	2.6	17	31	30	28
	5.5	3.0	1.5	7.9	11	47	17
$\Delta Co^* \Delta Co^*/\Delta OC$	-2.2	-1.8	-0.4	-2.7	-1.7	0.3	1.3
	-1.4	-1.1	-0.2	-1.2	-0.6	0.5	0.8
$\Delta Ni^* \Delta Ni^*/\Delta OC$	-15	-3.9	-2.3	-3.1	15	2.0	5.3
	-9.7	-2.3	-1.4	-1.4	5.2	3.2	3.2
$\Delta Cu^* \Delta Cu^*/\Delta OC$	-4.8	-4.6	-3.3	-2.3	5.2	-1.6	3.1
	-3.1	-2.7	-2.0	-1.0	1.8	-2.6	1.9
$\Delta Zn^* \Delta Zn^*/\Delta OC$	-17	-13	-9.8	-6.4	-2.1	-8.6	-4.5
	-11	-7.8	-5.9	-2.9	-0.7	-13	-2.7
$\Delta Se^* \Delta Se^*/\Delta OC$	0.13	-0.03	0.04	0.01	0.12	-0.43	0.02
	0.08	-0.02	0.02	0.00	0.04	-0.67	0.01
$\Delta Mo^* \Delta Mo^*/\Delta OC$	4.3	3.9	5.1	3.5	11	5.5	5.7
	2.8	2.3	3.1	1.6	4.0	8.6	3.5
$\Delta Cd^* \Delta Cd^*/\Delta OC$	0.46	0.43	0.22	0.59	1.5	1.4	1.3
	0.30	0.25	0.13	0.27	0.5	2.2	0.8
$\Delta Sb^* \Delta Sb^*/\Delta OC$	-0.1	-0.06	-0.05	0.09	0.59	-0.22	0.12
	-0.06	-0.04	-0.03	0.04	0.21	-0.35	0.07
$\Delta Re^* \Delta Re^*/\Delta OC$	20	16	20	26	59	25	27
	13	10	12	12	20	39	16
$\Delta U^* \Delta U^*/\Delta OC$	0.4	0.1	0.8	2.5	5.2	4.3	2.6
	0.3	0.04	0.5	1.2	1.8	6.7	1.6

Negative values indicate that X^* in PC464 is higher than in PC463. Note that $\Delta OC < 1$ blows up the $\Delta X^*/\Delta OC$ values for IP14.

et al., 1997; Von Rad et al., 1999). Their interpretation is based on the assumption that enrichment or depletion of elements can be used as proxy for the depth of the redox boundaries in the sediment that in turn depend on — among other variables — the BWO concentrations. For an unbiased interpretation, however, the total signals should be corrected not only for the contributions by the terrigenous ($\rightarrow X^*$) but also by biogenic fractions ($\rightarrow X^{**}$).

Piper and Isaacs (1995b) argued that the trace element content carried by organic matter is similar to the composition of average modern plankton. The X^{**} values, calculated after subtraction of this planktonic contribution (Eq. (A.6)), ideally should represent the contribution by diffusion only. This implies that differences between the X^{**} values in PC464 and in PC463 have to be explained in terms of differences in BWO conditions. Taking $X^{**}(463)$ as reference, the calculation (cf. Eq. (A.6)) of $X^{**}(464)$ can be made using the actual OM_{464} or the OM_{463} corrected for some loss in OM related to depth difference between these sites. The last scenario assumes that trace elements carried by OM are completely retained in the sediment during degradation, whereas in the first scenario elements carried by the diagenetically degraded

OM escape to the BW. Henceforth, the $X^{**}(464)$ values based on the corrected OM_{463} will be used. These values comprise enrichment by diffusion as well as by supply by excess MnO_x . The results are shown as bar graphs (Fig. 10). A general observation is that in Fig. 10b,c,e, a trend of increasing, stable and decreasing values for X^{**} similar to the trends in the baselines is present. This suggests that the peak heights are related to climatic changes and(or) sea level.

Fig. 10a shows the average values of *pyrite-S/OC* in the cores. All ratios are lower than the average value for normal marine sediment (~ 0.36), even lower than the envelope ratio (~ 0.6) indicative of transition of normal to euxinic sediments (Bernier, 1984). This means that even during these periods of relatively high accumulation of OM, no euxinic conditions developed in the water column. Schenau et al. (2002b) drew the same conclusion on the basis of sedimentary records on the continental margins off Oman (depth 516 m) and Pakistan (depth 1002 m) and in the central basin (depth 3570 m) of the northern Arabian Sea. For OM-rich intervals they found ratios < 0.3 , similar to the values for the relatively OM-rich insolation phases 4–16 (Fig. 10a). Profiles of PW concentrations in BC463 and BC464 show that suboxic

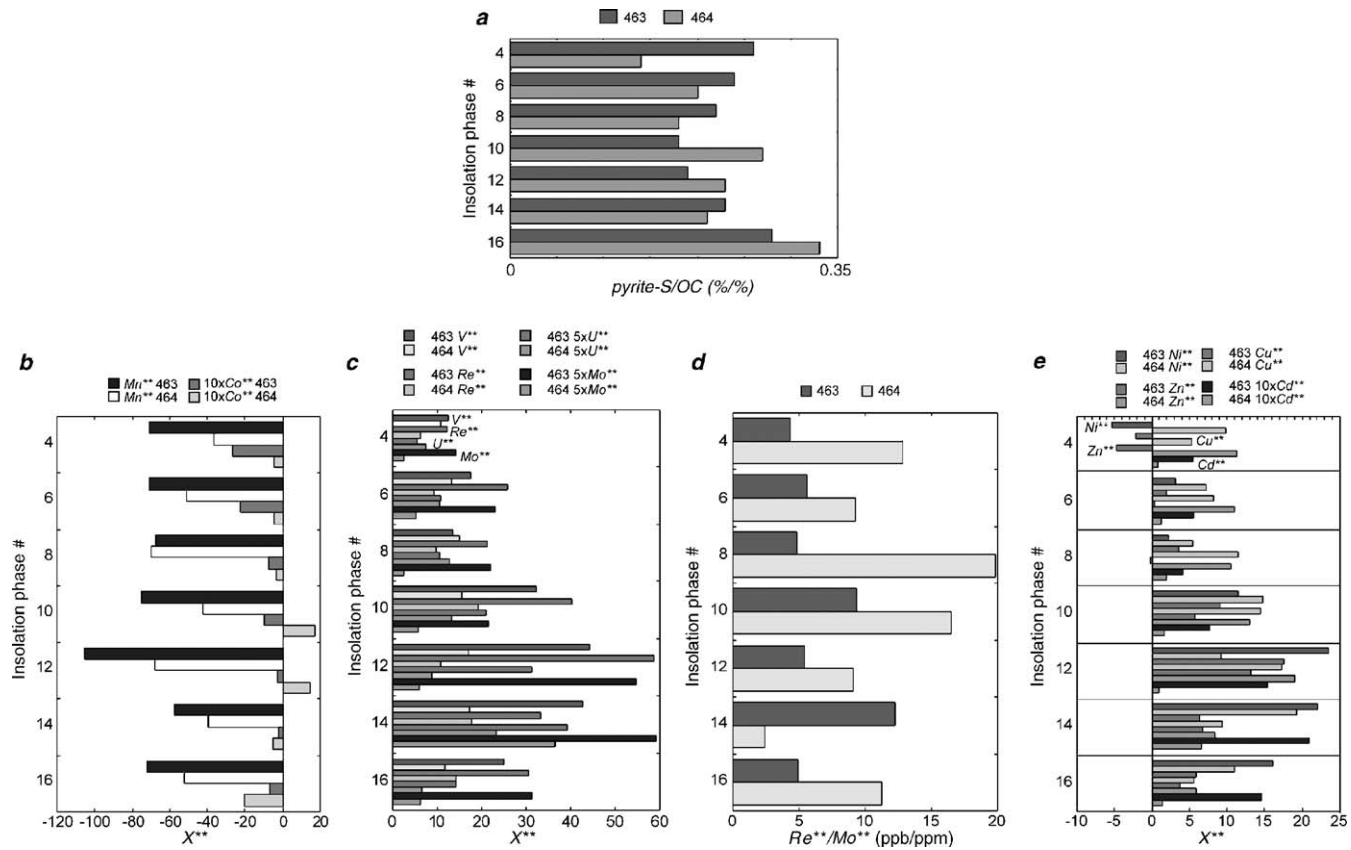


Fig. 10. Bargraphs of element ratios or contents (X^{**} means: corrected for lithogenous and planktonic contributions) in cores 463 and 464. a) $OC/pyrite-S$ (both in %); b) Mn^{**} and $(10\times)Co^{**}$ (both in ppm); c) V^{**} , Re^{**} , $(5\times)U^{**}$, $(5\times)Mo^{**}$ (except for Re^{**} in ppb, all in ppm); d) Re^{**}/Mo^{**} (as ppb/ppm); e) Ni^{**} , Cu^{**} , Zn^{**} , Cd^{**} (all in ppm).

conditions (reduction of MFO) prevail in the first 30 cm (Van der Weijden et al., 1999). The sulfate profiles in PWs of BC463, BC464 and PC463 show a linear decrease till a depth of approximately 3.5 m (in PC463; unpublished results) below the sediment–water interface (SWI) with ~25% of their BW value, after which the concentration remains approximately constant. The profiles in BC463 also show that, within an intense OMZ, dissolved Fe can partly escape into bottom water. When these features are representative for the records of the PCs, this means that anoxic sulfidic conditions leading to pyrite formation develop relatively deep below (>~30 cm; also indicated by the *Eh*-values mentioned in Section 5.2.3.) the SWI and that, during periods of very low BWO concentrations, pyrite formation is limited by partial loss of ferrous iron at and across the SWI.

A comparison of the Mn^{**} and Co^{**} values is shown in Fig. 10b. Relative to the terrigenous input, the sediments are lower in both elements. This shows that suboxic manganese reduction not only resulted in the loss of Mn at site 463, but also played a role in microbially mediated OM decomposition at site 464, confirming what was observed in BCs collected at the same sites (Van der Weijden et al., 1999). In general $Mn^{**}(463) < Mn^{**}(464)$, which is in line with the present extension of the OMZ. During IP4 and IP8 $Mn^{**}(464) < Mn^{**}(463)$, which might be explained by more efficient retention of Mn in a carbonate phase which formed as a consequence of sulfate reduction related alkalinity increases. During IP4–8, Co^{**} losses in PC463 are larger than in PC464, and during IP10 and IP12 there is a loss in Co^{**} in PC463 and a Co^{**} gain in PC464. Considering that Co is a common element in MnO_x (Clegg and Sarmiento, 1989; Brumsack, 2006), suboxic release of Co along with Mn dissolution is expected. Relative to PC463, the losses in Co^{**} in PC464 for IP4–12 are less compared to the difference in Mn^{**} . The concentration of Co in oceanic deep water is too small to explain Co enrichment by diffusion from bottom water into the sediment. More likely, Co carried to the sediment by MnO_x below the OMZ is retained in the sediment upon dissolution of its carrier phase.

Next on the *Eh* ladder and prone to enrichment by diffusion across the benthic boundary are the elements V, Re, U and Mo (Fig. 10c). For all IPs, Mo^{**} and Re^{**} in PC463 exceed those in PC464. Rhenium is preferentially enriched under suboxic and Mo under sulfidic conditions (Crusius et al., 1996; Morford and Emerson, 1999; Crusius and Thomson, 2000; Vorlicek and Helz, 2002; Vorlicek et al., 2004; Meyers et al., 2005; Algeo and Lyons, 2006). This implies that Re^{**}/Mo^{**} values potentially can be used to distinguish BWO conditions

(Crusius et al., 1996). With the exception of IP14, the ratios are higher in PC464 than PC463 (Fig. 10d), indicating that during IP14 the OMZ expanded to at least the depth of site 464. However, when interpreting Re^{**}/Mo^{**} ratios it must be realized that Re may become remobilized relative to Mo upon a change — even periodically — from suboxic to oxic BW (Crusius and Thomson, 2003).

Between the cores, almost no difference is observed for V^{**} and U^{**} during the periods IP4–8, while during the older IPs these elements are higher in PC463 than in PC464, again in agreement with more oxygen-depleted BW at site 463. At site 464, U^{**} is relatively high during IP14, but V^{**} is not.

Finally, the contents of the sulfophile elements Ni, Cu, Zn and Cd in both cores are compared (Fig. 10e). Negative values are caused by apparent overcorrection for lithogenic and(or) planktonic contributions.³ These elements are brought to the sediments largely by MFO and by biodebris and are immobilized under sulfidic conditions. (Böning et al., 2004). Overall, Cu^{**} and Zn^{**} have very similar values in both cores. For all IPs, $Zn^{**}(464) > Zn^{**}(463)$ and $Cd^{**}(463) > Cd^{**}(464)$, for IP4–10, Ni^{**} and Cu^{**} in PC464 are larger than in PC463, whereas during IP12–16 Ni^{**} is larger in PC463 than in PC464.

In summary, of the proxies for differences in depositional conditions tested in this section, only Mo^{**} , Re^{**} and Re^{**}/Mo^{**} can be interpreted unambiguously. A likely explanation is that the concentration gradients of these elements between BW and pore water are much larger than is the case for the other elements. The trace element data indicate that only during IP14 the OMZ expanded to the depth of station 464. Average element concentrations cannot be used to confirm suggested OMZ expansions (Den Dulk et al., 2000; Sinninghe Damsté et al., 2002) during IP6 and IP16. Although the normalization proposed here gives better insight in the processes involved in trace metal (re)distribution, averaging over relatively long periods is inevitably causing the loss of information on changes taking place on shorter time scales. OMZ expansions during IP6 and IP16 were relatively short lived, as is also evident from the short interval with laminated sediments during IP6, and did not affect trace metal inventories on a precession time scales.

³ In general, overcorrection by the adopted values for the lithogenic and biogenic fractions is possible, especially when the corrections are relatively large as is, for instance, the case for the values of element contents in plankton in combination with high OC contents.

6. Conclusions

- Major element contents indicate that the terrigenous fraction of sediment deposited at stations 463 and 464 at Murray Ridge has a very similar composition.
- Graphically derived trace-element contents of the terrigenous fraction of the cores are, generally, similar and compare well with values for standard shales; differences, especially for Mo, Re and U, are due to syngenetic and diagenetic imprints.
- When attributed to residual OM, the trace-element content of OM is, for most elements, higher than in planktonic debris.
- Trace-element records of *V*, *Ni*, *Cu*, *Zn*, *Se*, *Mo*, *Cd*, *Re* and *U* co-vary positively with *OC*, while negatively for *Mn* and *Co*. Their down-core profiles mostly display the highest amplitudes during periods of high insolation; more frequent smaller oscillations represent the dynamic character of the intensity and extent of the OMZ during the last 200 kyr.
- An expansion of the OMZ to, at least, the depth of station 464 (1500 m) relative to the current depth of the intense OMZ (~1150 m) is deduced from differences in *Re*^{**}, *Mo*^{**}, and *Re*^{**}/*Mo*^{**} between cores 463 and 464 only for the interval from 155 to 135 ka.

Acknowledgements

The Netherlands Indian Ocean Programme (1992/93) was sponsored by the Netherlands Geosciences Foundation, a section of the Netherlands Science Foundation (NWO). RV Tyro was our research vessel, W.J.M. van der Linden the chief scientist during leg D2 in the northern Arabian Sea. The government of Pakistan gave permission to work within its Exclusive Economic Zone of Pakistan. The program was carried out in close cooperation with the director and colleagues (A. A. Khan, M. Danish, G.M. Menon, and A.R. Tabrez) of the Pakistan National Institute of Oceanography (NIO) in Karachi. We thank Captain De Jong and his crew as well as the technicians J. Blom, E.B.M. Bos, R. Groenewegen, J. Schilling and M.A. Wijsman of the Royal Netherlands Institute for Sea Research (RNIOZ) for their indispensable help and support. Special thanks go to senior scientist W.J. Zachariasse for supervising the on-board core descriptions and sampling, and to L. Lourens for his support in developing and fine-tuning of the age model for the sedimentary record. M. van Alphen, A. van Dijk, G. Ittman, G. Nobbe, G. van het Veld and H. de Waard were involved in the sample preparation and analyses at the home laboratory. We owe many thanks to P. Böning and T. W. Lyons for critically reading an earlier version of the

manuscript. Their constructive comments and useful suggestions were of great help to improve the paper.

Appendix A. Use of normalization by Al content

The algebraic expression describing the relation between a normalized element concentration X and OM is

$$\left(\frac{X}{Al}\right)_{tot} = \frac{aX_{cl} + bX_{si} + cX_{ca} + dX_{OM} + eX_{hy}}{Al} \quad (A.1)$$

where the italicized symbols represent element contents in total sediment (tot), clays (cl), quartz + biogenic silica (si), carbonates (ca), organic matter (om) and hydrogenous or authigenic phases (hy), and a to e are the fractions of these sedimentary phases.

When the contributions by the detrital and marine fractions are considered separately, Eq. (A.1) can be recast into

$$\left(\frac{X}{Al}\right)_{tot} \approx \frac{X_{terrigenous}}{Al} + \frac{b^0 X_{si}^0 + cX_{ca} + (d/f)X_{OC} + eX_{hy}}{Al} \quad (A.2)$$

where b^0 represents the fraction and X^0 the trace element content of biogenic silica, and f is the conversion factor of the trace element content in OM into the content based on OC ($f=2.8$ when the Redfield ratio is adopted).

When X_{si}^0 , X_{ca} , and e are negligibly small, a plot of $(X/Al)_{tot}$ versus $OC (=df)$ or OC/Al intersects the ordinate at the value of $X_{terrigenous}/Al$. Subtraction of the $X_{terrigenous}/Al$ values (Table 2) from the actual ratios can be used to estimate the contributions of marine components to the trace element content (X^*). Eq. (A.1) can be recast as

$$\frac{X^*}{Al} = \left(\frac{X}{Al}\right)_{total} - \frac{X_{terrigenous}}{Al} = \frac{b^0 X_{si}^0 + cX_{ca} + dX_{OM} + eX_{hy}}{Al} \quad (A.3)$$

When b^0 and/or X_{si}^0 and X_{ca} are negligibly small, Eq. (A.3) can be simplified:

$$\frac{X^*}{Al} = X_{OM} \times \frac{d}{Al} + X_{hy} \times \frac{e}{Al} \quad (A.4)$$

or, multiplying each term with the concomitant Al for each sample,

$$X^* = dX_{OM} + eX_{hy} \quad (A.5)$$

Owing to the way in which X^*/Al was derived (Eq. (A.3)), a scattergram of X^* versus OC has its intersect with the origin. Since the hydrogenous enrichment of trace element X by diffusion across the water–sediment interface and immobilization in the sediment is a function of the OM content, the best-fit linear slope in the scattergram as well as the scatter of the data points around this slope depend on the contributions by both terms on the right-hand-side of Eqs. (A.4) and (A.5).

Finally, hydrogenous enrichment can be calculated from

$$eX_{hy} = X^* - dX_{OM} \quad (A6)$$

where reference values for plankton are adopted for X_{OM} .

Appendix B. Supplementary data

Supplementary data associated with this article can be found, in the online version, at [doi:10.1016/j.margeo.2006.05.013](https://doi.org/10.1016/j.margeo.2006.05.013).

References

- Algeo, T.J., Lyons, T.W., 2006. Mo–total organic carbon covariation in modern anoxic marine environments: implications for analysis of paleoredox and paleohydrographic conditions. *Paleoceanography* 21 (PA1016), 1–23.
- Altabet, M.A., Francois, R., Murray, D.W., Prell, W.L., 1995. Climate-related variations in denitrification in the Arabian Sea from sediment $^{15}N/^{14}N$ ratios. *Nature* 373, 506–509.
- Altabet, M.A., Higinson, M.J., Murray, D.W., 2002. The effect of millennium-scale changes in Arabian Sea denitrification on atmospheric CO_2 . *Nature* 415, 159–162.
- Berner, R.A., 1981. A new geochemical classification of sedimentary environments. *J. Sediment. Petrol.* 51, 359–365.
- Berner, R.A., 1984. Sedimentary pyrite formation: an update. *Geochim. Cosmochim. Acta* 48, 605–615.
- Böning, P., Brumsack, H.-J., Böttcher, M.E., Schnetger, B., Kriete, C., Kallmeyer, J., Borchers, S.L., 2004. Geochemistry of Peruvian near-surface sediments. *Geochim. Cosmochim. Acta* 68, 4429–4451.
- Böning, P., Cuypers, S., Grunwald, M., Schnetger, B., Brumsack, H.-J., 2005. Geochemical characteristics of Chilean upwelling sediments at $\sim 36^\circ S$. *Mar. Geol.* 220, 1–21.
- Brumsack, H.-J., 1989. Geochemistry of recent TOC-rich sediments from the Gulf of California and the Black Sea. *Geol. Rundsch.* 78, 851–882.
- Brumsack, H.-J., 2006. The trace metal content of recent organic carbon-rich sediments: implications for Cretaceous black shale formation. *Palaeogeogr. Palaeoclimatol. Palaeoecol.* 232, 344–361.
- Calvert, S.E., Pedersen, T.F., 1993. Geochemistry of Recent oxic and anoxic marine sediments: implications for the geological record. *Mar. Geol.* 113, 67–88.
- Calvert, S.E., Pedersen, T.F., Karlin, R.E., 2001. Geochemical and isotopic evidence for post-glacial paleoceanographic changes in Saanich Inlet, British Columbia. *Mar. Geol.* 174, 287–305.
- Chester, R., Berry, A.A., Murphy, K.J.T., 1991. The distribution of particulate atmospheric trace metals and mineral aerosols over the Indian Ocean. *Mar. Chem.* 34, 261–290.
- Clegg, S.L., Sarmiento, J.L., 1989. The hydrolytic scavenging of metal ions by marine particulate matter. *Prog. Oceanogr.* 23, 1–21.
- Collier, R., Edmond, J., 1984. The trace element geochemistry of marine biogenic particulate matter. *Prog. Oceanogr.* 13, 113–199.
- Colodner, D., Edmond, J., Boyle, E., 1995. Rhenium in the Black Sea: comparison with molybdenum and uranium. *Earth Planet. Sci. Lett.* 131, 1–15.
- Crusius, J., Thomson, J., 2000. Comparative behavior of authigenic Re, U, and Mo during reoxidation and subsequent long-term burial in marine sediments. *Geochim. Cosmochim. Acta* 64, 2233–2242.
- Crusius, J., Thomson, J., 2003. Mobility of authigenic rhenium, silver, and selenium during postdepositional oxidation in marine sediments. *Geochim. Cosmochim. Acta* 67, 265–274.
- Crusius, J., Calvert, S.E., Pedersen, T.F., Sage, D., 1996. Rhenium and molybdenum enrichments in sediments as indicators of oxic, suboxic and sulfidic conditions of deposition. *Earth Planet. Sci. Lett.* 145, 65–78.
- Dean, W.E., Gardner, J.V., Piper, D.Z., 1997. Inorganic geochemical indicators of glacial–interglacial changes in productivity and anoxia on the California continental margin. *Geochim. Cosmochim. Acta* 61, 4507–4518.
- Dean, D.E., Piper, D.Z., Peterson, L.C., 1999. Molybdenum accumulation in Cariaco basin sediment over the past 24 k.y.: a record of water-column anoxia and climate. *Geology* 27, 507–510.
- Den Dulk, M., Reichart, G.J., Van Heyst, S., Zachariasse, W.J., Van der Zwaan, G.J., 2000. Benthic foraminifera as proxies of organic matter flux and bottom water oxygenation? A case history from the northern Arabian Sea. *Palaeogeogr. Palaeoclimatol. Palaeoecol.* 161, 337–359.
- Fisher, N.S., Went, M., 1993. The release of trace elements by dying marine phytoplankton. *Deep-Sea Res.* 1 40, 671–694.
- Fontugne, M.R., Calvert, S.E., 1992. Late Pleistocene variability of the carbon isotope composition of organic matter in the eastern Mediterranean: monitor of changes in carbon sources and atmospheric CO_2 concentrations. *Paleoceanography* 7, 1–20.
- Fowler, S.W., 1977. Trace elements in zooplankton particulate products. *Nature* 269, 51–53.
- Francois, R., 1988. A study on the regulator of the concentrations of some trace metals (Rb, Sr, Zn, Pb, Cu, V, Cr, Ni, Mn and Mo) in Saanich Inlet sediments, British Columbia, Canada. *Mar. Geol.* 83, 285–308.
- Gromet, L.P., Dymek, R.F., Haskin, L.A., Korotev, R.L., 1984. The “North American shale composite”: is compilation, major and trace element characteristics. *Geochim. Cosmochim. Acta* 48, 2469–2482.
- Hlawatsch, S., Garbe-Schönberg, C.D., Lechtenberg, F., Manceau, A., Tamura, N., Kulik, D.A., Kersten, M., 2002. Trace metal fluxes to ferromanganese nodules from the western Baltic Sea as a record for long-term environmental changes. *Chem. Geol.* 182, 697–709.
- Hong, J., Calmano, W., Förstner, U., 1995. Interstitial waters. In: Salbu, B., Steinnes, E. (Eds.), *Trace Elements in Natural Waters*. CRC Press, Boca Raton, pp. 117–150.
- Jacobs, L., Emerson, S., Huested, S.S., 1987. Trace metal geochemistry in the Cariaco Trench. *Deep-Sea Res.* 34, 965–981.
- Laskar, J., Joutel, F., Boudin, F., 1993. Orbital, precessional and insolation quantities for the Earth from -20 Myr to $+10$ Myr. *Astron. Astrophys.* 270, 522–533.
- Lourens, L.J., Antonarakou, A., Hilgen, F.J., Van Hoof, A.A.M., Vergnaud-Grazzini, C., Zachariasse, W.J., 1996. Evaluation of the Pliocene–Pleistocene astronomical timescale. *Paleoceanography* 11, 391–413.
- Lyons, T.W., Werne, J.P., Hollander, D.J., Murray, R.W., 2003. Contrasting sulfur geochemistry and Fe/Al and Mo/Al ratios across the last oxic-to-anoxic transition in the Cariaco Basin, Venezuela. *Chem. Geol.* 195, 131–157.

- Meyers, S.R., Sageman, B.B., Lyons, T.W., 2005. Organic carbon burial rate and the molybdenum proxy: theoretical framework and application to Cenomanian–Turonian oceanic anoxic event 2. *Paleoceanography* 20 (PA2002) (19 pp.).
- Morford, J.L., Emerson, S., 1999. The geochemistry of redox sensitive trace metals in sediments. *Geochim. Cosmochim. Acta* 63, 1735–1750.
- Morford, J.L., Russell, A.D., Emerson, S., 2001. Trace metal evidence for changes in the redox environment associated with the transition from terrigenous clay to diatomaceous sediment, Saanich Inlet, BC. *Mar. Geol.* 174, 355–369.
- Nameroff, T.J., Balistrieri, L.S., Murray, J.W., 2002. Suboxic trace metal geochemistry in the eastern tropical North Pacific. *Geochim. Cosmochim. Acta* 66, 1139–1158.
- Olson, D.B., Hitchcock, G.L., Fine, R.A., Warren, B.A., 1993. Maintenance of the low-oxygen layer in the central Arabian Sea. *Deep-Sea Res.*, II 40, 673–685.
- Piper, D.Z., 1994. Seawater as the source of minor elements in black shales, phosphorites and other sedimentary rocks. *Chem. Geol.* 114, 95–114.
- Piper, D.Z., Dean, W.E., 2003. Trace-Element Deposition in the Cariaco Basin, Venezuela Shelf, Under Sulfate-Reducing Conditions — a History of the Local Hydrography and Global Climate, 20 ka to the Present. U.S. Geol. Soc., Reston, Virginia. 41 pp.
- Piper, D.Z., Isaacs, C.M., 1995a. Minor elements in Quaternary sediment from the Sea of Japan: a record of surface-water productivity and intermediate-water redox conditions. *GSA Bull.* 107, 54–67.
- Piper, D.Z., Isaacs, C.M., 1995b. Geochemistry of Minor Elements in the Monterey Formation, California: Seawater Chemistry of Deposition. U.S. Geol. Survey Prof. Paper 1566. United States Government Printing Office, Washington. 41 pp.
- Piper, D.Z., Isaacs, C.M., 1996. Instability of bottom-water redox conditions during accumulation of Quaternary sediment in the Japan Sea. *Paleoceanography* 11, 171–190.
- Reichart, G.J., 1997. Late Quaternary variability of the Arabian Sea monsoon and oxygen minimum zone. PhD thesis Utrecht University. *Geologica Ultraiectina* 154: 145–151.
- Reichart, G.J., Brinkhuis, H., 2003. Late Quaternary *Protoperidinium* cysts as indicators of paleoproductivity in the northern Arabian Sea. *Mar. Micropaleontol.* 49, 303–315.
- Reichart, G.J., Lourens, L.J., Zachariasse, W.J., 1998. Temporal variability in the northern Arabian Sea Oxygen Minimum Zone (OMZ) during the last 225 000 years. *Paleoceanography* 13, 607–621.
- Reichart, G.J., Nortier, J., Versteegh, G., Zachariasse, W.J., 2002. Periodical breakdown of the Arabian Sea oxygen minimum zone caused by deep convective mixing. In: Clift, P.D., Kroon, D., Gaedicke, C., Craig, J. (Eds.), *The Tectonic and Climatic Evolution of the Arabian Sea Region*. Special Publication, vol. 195. Geological Society, London, pp. 407–419.
- Reichart, G.J., Den Dulk, M., Visser, H.J., Van der Weijden, C.H., Zachariasse, W.J., 1997. A 225 kyr record of dust supply, paleoproductivity and the oxygen minimum zone from the Murray Ridge (northern Arabian Sea). *Palaeogeogr. Palaeoclimatol. Palaeoecol.* 134, 149–169.
- Reichart, G.J., Brinkhuis, H., Huiskamp, F., Zachariasse, W.J., 2004. Hyperstratification following glacial overturning events in the northern Arabian Sea. *Paleoceanography* 19 (PA2013) (8 pp.).
- Russell, A.D., Morford, J.L., 2001. The behavior of redox-sensitive metals across a laminated–massive–laminated transition in Saanich Inlet, British Columbia. *Mar. Geol.* 174, 341–354.
- Saager, P.M., De Baar, H.J.W., Burkill, P.H., 1989. Manganese and iron in Indian Ocean waters. *Geochim. Cosmochim. Acta* 53, 2259–2267.
- Saager, P.M., De Baar, H.J.W., Howland, R.J., 1992. Cd, Zn, Ni and Cu in the Indian Ocean. *Deep-Sea Res.* 39, 9–35.
- Schenau, S.J., Reichart, G.J., De Lange, G.J., 2002a. Oxygen minimum zone controlled Mn redistribution in Arabian Sea sediments during the Late Quaternary. *Paleoceanography* 17 (4), 10-1–10-12.
- Schenau, S.J., Passier, H.F., Reichart, G.J., De Lange, G.J., 2002b. Sedimentary pyrite formation in the Arabian Sea. *Mar. Geol.* 185, 393–402.
- Schulte, S., Rostek, F., Bard, E., Rullkötter, J., Marchal, O., 1999. Variations of oxygen minimum and primary productivity recorded in sediments of the Arabian Sea. *Earth Planet. Sci. Lett.* 173, 205–221.
- Schulz, H., Von Rad, U., Erlenkeuser, H., 1998. Correlation between Arabian Sea and Greenland climate oscillations of the past 110 000 years. *Nature* 393, 54–57.
- Shaw, T.J., Gieskes, J.M., Jahnke, R.A., 1990. Early diagenesis in differing depositional environments: the response of transition metals in pore water. *Geochim. Cosmochim. Acta* 54, 1233–1246.
- Sinninghe Damsté, J.S., Rijpstra, W.E., Reichart, G.J., 2002. The influence of oxic degradation on the sedimentary biomarker record. II. Evidence from Arabian Sea sediments. *Geochim. Cosmochim. Acta* 65, 2737–2754.
- Sirocko, F., Garbe-Schönberg, D., Devey, C., 2000. Processes controlling trace element geochemistry of Arabian Sea sediments during the last 25 000 years. *Glob. Planet. Change* 26, 217–303.
- Taylor, S.R., McLennan, S.M., 1985. The continental crust: its composition and evolution. An examination of the geochemical record preserved in sedimentary rocks. *Geoscience Texts*. Blackwell Scientific Publications, Oxford, pp. 9–56.
- Thomson, J., Nixon, S., Croudace, I.W., Pedersen, T.F., Brown, L., Cook, G.T., Mackenzie, A.B., 2001. Redox-sensitive element uptake in north-east Atlantic Ocean sediments (Benthic Boundary Layer Experiment sites). *Earth Planet. Sci. Lett.* 184, 535–547.
- Turekian, K.K., Wedepohl, K.H., 1961. Distribution of the elements in some major units of the Earth's crust. *Geol. Soc. Amer. Bull.* 72, 175–192.
- Van Bennekom, A.J., Hiehle, M.A., 1994. CTD operations and calibrations during legs D1, D2 and D3 of the Netherlands Indian Ocean Programme. In: Van der Linden, W.J.M., Van der Weijden, C.H. (Eds.), *Geological Study of the Arabian Sea*. Netherlands Geosciences Foundation, The Hague, pp. 37–66.
- Van der Weijden, A.J., Van der Weijden, C.H., 2002. Silica fluxes and opal dissolution rates in the northern Arabian Sea. *Deep-Sea Res.*, I 49, 157–173.
- Van der Weijden, C.H., Reichart, G.J., Visser, H.J., 1999. Enhanced preservation of organic matter in sediments deposited within the oxygen minimum zone in the northeastern Arabian sea. *Deep-Sea Res.*, I 46, 807–830.
- Von Rad, U., Schulz, H., Riech, V., Den Dulk, M., Berner, U., Sirocko, F., 1999. Multiple monsoon-controlled breakdown of oxygen-minimum conditions during the past 30 000 years documented in laminated sediments off Pakistan. *Palaeogeogr. Palaeoclimatol. Palaeoecol.* 152, 129–161.
- Vorlicek, T.P., Helz, G.R., 2002. Catalysis by mineral surfaces: implications for Mo geochemistry in anoxic environments. *Geochim. Cosmochim. Acta* 66, 3679–3692.
- Vorlicek, T.P., Kahn, M.D., Kasuya, Y., Helz, G.R., 2004. Capture of molybdenum in pyrite-forming sediments: role of ligand-induced reduction by polysulfides. *Geochim. Cosmochim. Acta* 68, 547–556.
- Yarincik, K.M., Murray, R.W., Peterson, L.C., Haug, G.H., 2000. Oxygenation history of bottom waters in the Cariaco Basin,

- Venezuela, over the past 578,000 years: results from redox-sensitive metals (Mo, V, Mn, and Fe). *Paleoceanography* 15, 593–604.
- Wedepohl, K.H., 1971. Environmental influences on the chemical composition of shales and clays. In: Ahrens, L.H., Press, F., Runcom, S.K., Urey, H.C. (Eds.), *Physics and Chemistry of the Earth*, vol. 8. Pergamon Press, Oxford, United Kingdom, pp. 307–333.
- Wignall, P.B. (1994). *Black shales*. Oxford Monographs on Geology and Geophysics. Oxford Science Publications. Clarendon Press, Oxford, United Kingdom. pp. 39–48.